European Radiology (2022) 32:5679–5687
https://doi.org/10.1007/s00330-022-08638-1

IMAGING INFORMATICS AND ARTIFICIAL INTELLIGENCE

Accelerating susceptibility-weighted imaging with deep learning by complex-valued convolutional neural network (ComplexNet): validation in clinical brain imaging

Caohui Duan[1] · Yongqin Xiong[1] · Kun Cheng[1] · Sa Xiao[2] · Jinhao Lyu[1] · Cheng Wang[2] · Xiangbing Bian[1] · Jing Zhang[1] · Dekang Zhang[1] · Ling Chen[2] · Xin Zhou[3] · Xin Lou[1]

Received: 17 August 2021 / Revised: 15 December 2021 / Accepted: 11 January 2022 / Published online: 19 February 2022

Abstract

Objectives Susceptibility-weighted imaging (SWI) is crucial for the characterization of intracranial hemorrhage and mineralization, but has the drawback of long acquisition times. We aimed to propose a deep learning model to accelerate SWI, and evaluate the clinical feasibility of this approach.

Methods A complex-valued convolutional neural network (ComplexNet) was developed to reconstruct high-quality SWI from highly accelerated k-space data. ComplexNet can leverage the inherently complex-valued nature of SWI data and learn richer representations by using complex-valued network. SWI data were acquired from 117 participants who underwent clinical brain MRI examination between 2019 and 2021, including patients with tumor, stroke, hemorrhage, traumatic brain injury, etc. Reconstruction quality was evaluated using quantitative image metrics and image quality scores, including overall image quality, signal-to-noise ratio, sharpness, and artifacts.

Results The average reconstruction time of ComplexNet was 19 ms per section (1.33 s per participant). ComplexNet achieved significantly improved quantitative image metrics compared to a conventional compressed sensing method and a real-valued network with acceleration rates of 5 and 8 ($p < 0.001$). Meanwhile, there was no significant difference between fully sampled and ComplexNet approaches in terms of overall image quality and artifacts ($p > 0.05$) at both acceleration rates. Furthermore, ComplexNet showed comparable diagnostic performance to the fully sampled SWI for visualizing a wide range of pathology, including hemorrhage, cerebral microbleeds, and brain tumor.

Conclusions ComplexNet can effectively accelerate SWI while providing superior performance in terms of overall image quality and visualization of pathology for routine clinical brain imaging.

Key Points

- *The complex-valued convolutional neural network (ComplexNet) allowed fast and high-quality reconstruction of highly accelerated SWI data, with an average reconstruction time of 19 ms per section.*
- *ComplexNet achieved significantly improved quantitative image metrics compared to a conventional compressed sensing method and a real-valued network with acceleration rates of 5 and 8 ($p < 0.001$).*
- *ComplexNet showed comparable diagnostic performance to the fully sampled SWI for visualizing a wide range of pathology, including hemorrhage, cerebral microbleeds, and brain tumor.*

Keywords Artificial intelligence · Brain · Deep learning · Magnetic resonance imaging

✉ Xin Lou
louxin@301hospital.com.cn

[1] Department of Radiology, Chinese PLA General Hospital, Beijing 100853, People's Republic of China

[2] Department of Neurosurgery, Chinese PLA General Hospital, 28 Fuxing Road, Beijing 100853, People's Republic of China

[3] Key Laboratory of Magnetic Resonance in Biological Systems, State Key Laboratory of Magnetic Resonance and Atomic and Molecular Physics, National Center for Magnetic Resonance in Wuhan, Wuhan Institute of Physics and Mathematics, Innovation Academy for Precision Measurement Science and Technology, Chinese Academy of Sciences–Wuhan National Laboratory for Optoelectronics, Wuhan 430071, People's Republic of China

Abbreviations

CMBs	Cerebral microbleeds
CNN	Convolutional neural network
ComplexNet	Complex-valued convolutional neural network
CS	Compressed sensing
GRE	Gradient echo
MARS	Microbleed Anatomical Rating Scale
PSNR	Peak signal-to-noise ratio
R	Acceleration rate
RealNet	real-valued convolutional neural network
SSIM	Structural similarity
SWI	Susceptibility-weighted imaging

Introduction

Susceptibility-weighted imaging (SWI) is a powerful tool for clinical brain imaging due to its particular sensitivity for deoxygenated blood and intracranial mineral deposition [1]. Consequently, SWI has been widely applied for imaging a broad range of pathology, including intracranial hemorrhage, cerebral microbleeds (CMBs), traumatic brain injury, hemorrhagic or calcified neoplasms, and neurodegenerative disorders associated with mineralization or brain iron accumulation [1–3]. However, SWI requires a long echo time to build up the phase contrast [4], which necessitates relatively long acquisition times that may contribute to motion artifacts and patient anxiety [1, 4]. Long acquisition time also limits the spatial resolution and slice thickness in routine clinical SWI.

SWI typically uses a T2*-weighted gradient echo (GRE) sequence for data acquisition, and then combines both magnitude and phase information to enhance contrast in T2*-weighted images [1, 4]. To accelerate SWI data acquisition, one effective approach is to undersample k-space data and then reconstruct it using additional information [4, 5]. Traditionally, reconstructing images from undersampled data involves leveraging techniques such as parallel imaging and compressed sensing (CS) [6, 7]. However, parallel imaging suffers from noise amplification at high acceleration rates (*R*), and CS reconstruction is computationally expensive and typically requires empirical tunning of regularization parameters [5], which is challenging to deploy in real clinical applications.

Recently, deep learning has gained great interest for reconstructing undersampled MRI data, providing improved performance in both reconstruction quality and speed [8–10]. Even though MRI data are inherently complex-valued in nature, most of deep learning–based reconstruction methods employ real-valued operations and representations by treating real and imaginary components as two independent channels [6, 11]. Nevertheless, such strategy potentially alters the phase information during reconstruction because different weights are applied to the two input channels [6]. To faithfully reconstruct both MR magnitude and phase images, a few studies have proposed to apply complex-valued networks to MRI reconstruction [6, 11–14]. In particular, Cole et al demonstrated that complex-valued networks can enable superior undersampled MRI reconstruction and phase-based applications compared to real-valued networks [6].

The purpose of the present study was to develop a novel deep complex-valued convolutional neural network (ComplexNet) for fast and accurate reconstruction of highly accelerated SWI data, and investigate its performance in terms of reconstruction quality and visualization of pathology in clinical brain imaging.

Materials and methods

Study participants

This study was approved by the Institutional Review Board and informed written consent was obtained. GRE (SWI) data were prospectively acquired from participants undergoing a clinical brain MRI examination between July 2019 and May 2021. There were no exclusion criteria beyond those for routine clinical MRI.

Data acquisition and preprocessing

The GRE data were acquired on a 3.0-T scanner (Discovery MR750; GE Healthcare) equipped with an 8-channel brain coil, using an enhanced T2*-weighted angiography sequence. Relevant imaging parameters included repetition time = 30.6 ms, echo time with 12 echoes ranging from 3.1 to 27.6 ms, matrix size = 256 × 256, field of view = 240 × 240 mm^2, flip angle = 12°, bandwidth = 62.5 kHz, slice thickness = 2 mm, number of slices = 60 to 80, twofold undersampling in the first phase-encoding direction, and a total acquisition time of approximately 3 min.

The GRE data were reconstructed directly on the MR scanner and were saved as magnitude and phase images into DICOM files. The magnitude and phase images were then combined as complex images that were used as a "fully sampled" reference in the network training. Because SWI is usually generated from single-echo GRE acquisition [15], the GRE data with echo time = 23.0 ms [3] were selected to train and evaluate ComplexNet for SWI application. The dataset was split into 2D axial slices of 70 participants for training, 12 participants for validation, and 35 participants for testing. It should be noted that there is no data overlapping between the training dataset, validation dataset, and test dataset.

The volume data of each participant was split into axial slices of size 256 × 256, with each slice serving as a separate training example. The undersampled data were generated by retrospectively undersampling the reference k-space data using a sampling pattern library consisting of 3000 different two-dimensional variable-density random undersampling

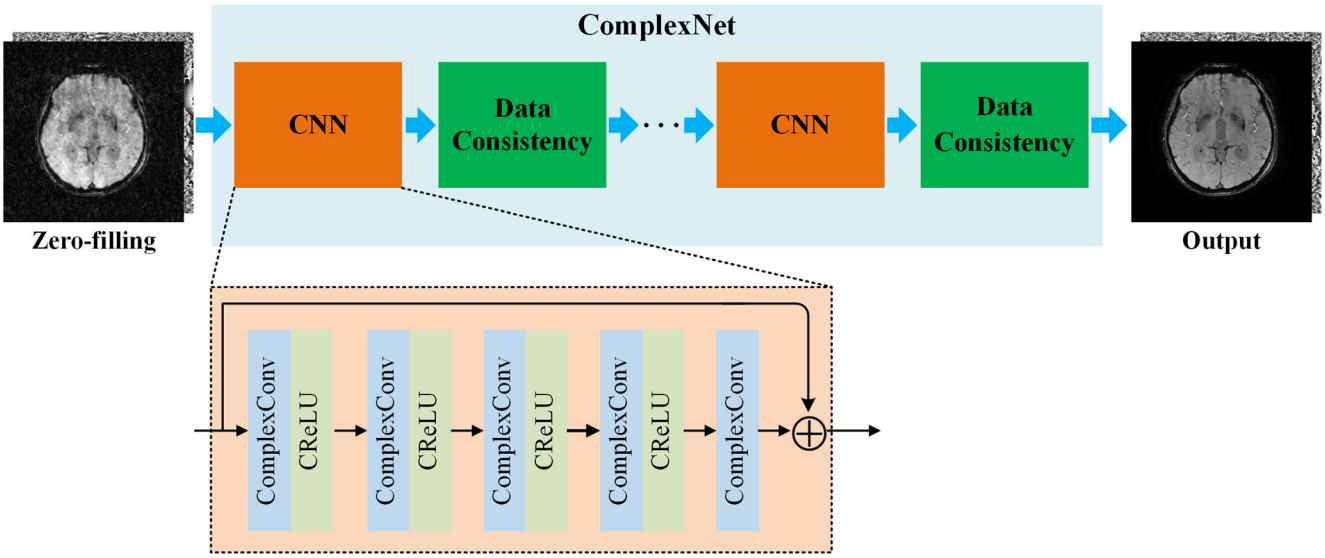

Fig. 1 The scheme of the ComplexNet for reconstruction of highly accelerated GRE data. ComplexNet takes zero-filling images as input, and outputs high-quality reconstruction of GRE data. *CNN*, convolutional neural network; *ComplexNet*, complex-valued convolutional neural network; *ComplexConv*, complex convolutional layer; *CReLU*, complex rectified linear unit; *GRE*, gradient echo; *SWI*, susceptibility-weighted imaging

masks [16]. For each undersampling mask, a region of 20 × 20 was consistently fully sampled in the k-space center, and two acceleration rates (R = 5 and R = 8) were investigated. In a prospective way, the scan time could be reduced by approximately 80% (144 s) for R = 5, and 87.5% (157.5 s) for R = 8 compared to the fully sampled acquisition.

Network architecture

The proposed ComplexNet for reconstruction of highly undersampled GRE data is shown in Fig. 1, which forms an unrolled network architecture by repeating convolutional neural network (CNN) modules and data consistency layers several times [17]. We adopt the complex residual network as the CNN modules to represent complex GRE data and accurately recover both MR magnitude and phase images. Furthermore, each CNN module is followed by a data consistency layer to ensure consistency with the physically measured k-space data [18]. In each reconstruction module, four complex convolutional layers, with a 3 × 3 kernel size and 128 feature maps, are sequentially applied to extract abundant features. Then, a complex convolutional layer with a 1 × 1 kernel size is used to reconstruct the residual images. Each complex convolutional layer, except for the last layer, is followed by a complex-valued activation function [6]. The details of the network architecture are described in Supplementary material.

Implementation and training

ComplexNet was implemented using the TensorFlow package (version R2.5; https://tensorflow.google.org). All training and testing were performed on a desktop computer with an Intel Xeon® Gold 6226R CPU, 128 GB RAM, and an RTX 3090 GPU. During the training process, the network weights were initialized using a previously described method [12] and were optimized using the Adam algorithm [19], with a fixed learning rate of 0.0002, β_1 = 0.9, β_2 = 0.999, and batch size of 8. The training parameters were optimized on the validation dataset (see details in Supplementary material). The mean-squared error between the reconstructed results and the reference images was chosen as the loss function. The total training time was approximately 24 h for 200 epochs.

Once the training process was completed, the parameters of the ComplexNet were fixed and can be adopted for effective and direct transformation of new accelerated GRE data to the corresponding reconstruction results. After obtaining high-quality reconstruction of the GRE data, standard SWI processing was performed to produce high-pass filtered phase images and associated SWI images using SEPIA software [20].

Evaluation

ComplexNet was compared with a conventional CS-MRI method and a real-valued convolutional neural network (RealNet) with the same unrolled architecture as ComplexNet, using the standard real-valued activation function and convolutional layers. CS-MRI reconstruction was implemented in MATLAB (version 2018a; Mathworks) based on the wavelet sparsifying transform and total variation regularization [21]. RealNet was implemented on TensorFlow using fewer feature maps to match the number of parameters of ComplexNet [6].

The reconstruction results of GRE data were evaluated using two quantitative metrics: peak signal-to-noise ratio (PSNR) and structural similarity (SSIM) [22]. PSNR was

evaluated on complex-valued images to account for differences in both magnitude and phase images, and SSIM was only evaluated on the magnitude images [6]. In addition, the SWI images with blinded reconstruction information were individually evaluated by two experienced radiologists (with 5 and 7 years of experience in brain MRI interpretation) in terms of overall image quality, SNR, sharpness, and artifacts with scores ranging from 1 to 5 [8]. Scoring criteria are shown in Supplementary Table 1.

To provide a quantitative assessment of the diagnostic performance of ComplexNet, the number and location of the CMBs were also evaluated by the two radiologists independently with blinded reconstruction information [2, 23]. The detection and counting of the CMBs were based on the Microbleed Anatomical Rating Scale (MARS) [24]. Cases with gross structural lesions that may limit the reliability of the CMB counts were excluded [2]

Statistical analysis

Paired two-tailed Student's *t* tests were performed to compare the quantitative image metrics between the different reconstruction methods. McNemar tests were used to compare the dichotomous variables (the presence of CMBs), and the Wilcoxon signed rank tests were used to compare the ordinal variables (image quality scores and the number of CMBs) between the fully sampled and ComplexNet approaches [2]. To assess noninferiority of ComplexNet to the fully sampled method, a two-sided 95% confidence interval for the difference in image quality scores between the two methods was calculated [25]. The noninferiority margin for the difference was set as − 0.5 score points according to a previous study [26].

The interobserver agreement for the presence and numbers of CMBs on the ComplexNet and fully sampled approaches was assessed by using the kappa value and intraclass correlation coefficient, respectively. The kappa and intraclass correlation coefficient results were interpreted according to a previous study [23]. All statistical analyses were performed using SPSS (version 24.0; IBM), and statistical significance was set at $p < 0.05$.

Results

Clinical characteristics of the study participants are summarized in Table 1. The SWI data were acquired from 117 participants (mean age, 53 years ± 17; 73 men), including patients with tumor, stroke, Parkinson's disease, dizziness, hemorrhage, traumatic brain injury, and other conditions.

Figure 2 shows representative SWI images obtained using different reconstruction methods at $R = 5$ (top row) and $R = 8$ (bottom row) in a 40-year-old man with multiple cerebral microbleeds. The corresponding magnitude and phase images are provided in Supplementary Fig. 2. It can be seen that the zero-filling images show severe artifacts and blurred structures due to sub-Nyquist sampling. Although the CS-MRI reconstruction can remove the artifacts to some extent, it leads to noticeable smooth patterns and loss of image details, as indicated by the golden arrows in Fig. 2(b1 and b2). Nevertheless, the deep learning–based methods (i.e., RealNet and ComplexNet) generate nearly artifact-free SWI images with well-preserved sharpness and structures comparable to the fully sampled images, and ComplexNet achieves superior quantitative metrics than RealNet. Average reconstruction time is 19 ms per section (1.33 s per participant) for ComplexNet in TensorFlow on the RTX 3090 GPU.

Table 1 Clinical characteristics of the study participants

Variable	Value
No. of patients	117
Age (years)*	53 ± 17
Sex	
Male	73 (62)
Female	44 (38)
Clinical indication for MRI	
Tumor	24 (20.5)
Stroke	18 (15.4)
Healthy	14 (12.0)
Parkinson's disease	11 (9.4)
Dizziness	8 (6.8)
Hemorrhage	7 (6.0)
Traumatic brain injury	5 (4.3)
Other	30 (25.6)

Note: Unless otherwise specified, data are the number of participants, with percentages in parentheses

*Data are means ± standard deviations

Table 2 summarizes the mean PSNR and SSIM values obtained using different algorithms at $R = 5$ and $R = 8$ for all the test data. Mean PSNR and SSIM values for ComplexNet range from 32.65 ± 2.30 and 0.9156 ± 0.0258 at $R = 8$ to 35.26 ± 2.3 and 0.9377 ± 0.0186 at $R = 5$, respectively. For both $R = 5$ and $R = 8$, ComplexNet and RealNet achieve significantly better image quality than CS-MRI ($p < 0.001$). Moreover, ComplexNet consistently outperforms RealNet at both acceleration rates ($p < 0.001$).

Figure 3 summarizes the results of image quality scores for the fully sampled and ComplexNet approaches at $R = 5$ and $R = 8$. There is no significant difference between fully sampled and ComplexNet approaches at $R = 5$ in terms of all the evaluation criteria, including overall image quality ($p = 0.47$; mean score ± standard deviation, 4.4 ± 0.4 for ComplexNet and 4.5 ± 0.6 for the fully sampled approach), SNR ($p = 0.11$; mean score, 3.9 ± 0.4 for ComplexNet and 4.0 ± 0.7 for the fully

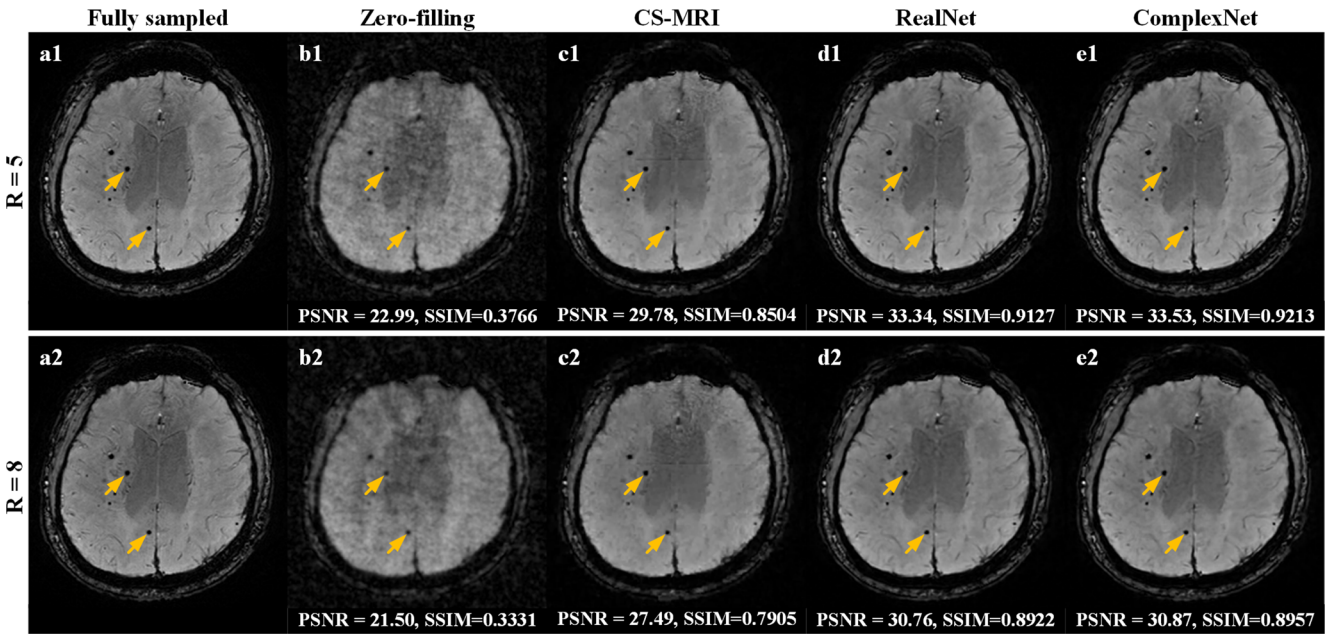

Fig. 2 Representative SWI images in a 40-year-old man with multiple cerebral microbleeds for comparison of different reconstruction methods at $R = 5$ (top row) and $R = 8$ (bottom row). ComplexNet showed the highest image quality with well-preserved sharpness and clear visualization of scattered microbleeds in the right lateral ventricle (golden arrows). *CS-MRI*, compressed sensing MRI; *PSNR*, peak signal-to-noise ratio; *R*, acceleration rate; *RealNet*, real-valued convolutional neural network; *SSIM*, structure similarity

sampled approach), sharpness ($p = 0.19$; mean score, 4.0 ± 0.3 for ComplexNet and 4.2 ± 0.6 for fully sampled approach), and artifacts ($p = 0.54$; mean score, 3.9 ± 0.3 for ComplexNet and 3.8 ± 0.7 for the fully sampled approach). At $R = 8$, ComplexNet achieves slightly lower scores than the fully sampled approach in terms of SNR ($p = 0.01$; mean score, 3.8 ± 0.4 for ComplexNet) and sharpness ($p = 0.03$; mean score, 4.0 ± 0.4 for ComplexNet), with no significant difference in overall image quality ($p = 0.08$; mean score, 4.3 ± 0.7 for ComplexNet) and artifacts ($p = 0.59$; mean score, 3.9 ± 0.5 for ComplexNet).

The results of noninferiority testing are shown in Supplementary Fig. 3. Since the lower limits of the two-sided 95% confidence intervals for the difference are all above the predefined noninferiority margin (− 0.5 score points), the noninferior of ComplexNet to the fully sampled method in terms of image quality scores was inferred.

Representative SWI images comparing the fully sampled and ComplexNet approaches in the presence of pathologic diseases are shown in Figs. 4 and 5. In Fig. 4, ComplexNet shows a similar diagnostic image quality as the fully sampled approach for visualization of pathology, including extensive susceptibility effect in traumatic brain injury, ring-like susceptibility effect in cerebral hemorrhage, and scattered foci of susceptibility effect in arteriovenous malformation. SWI images in Fig. 5(b1–b3) show internal architecture and hemorrhages within the brain tumor, which could be also clearly captured in the SWI images obtained using ComplexNet at both $R = 5$ (Fig. 5(c1–c3)) and $R = 8$ (Fig. 5(d1–d3)).

Table 2 Comparison of quantitative image metrics on test datasets with different reconstruction methods at $R = 5$ and $R = 8$

Methods	$R = 5$		$R = 8$	
	PSNR	SSIM	PSNR	SSIM
Zero-filling	24.24 ± 2.1	0.3782 ± 0.0509	23.14 ± 2.09	0.3485 ± 0.0491
CS-MRI	31.42 ± 2.41	0.8708 ± 0.0628	28.85 ± 2.42	0.7698 ± 0.0943
RealNet	35.10 ± 2.2	0.9282 ± 0.0193	32.53 ± 2.33	0.9129 ± 0.0270
ComplexNet	**35.26 ± 2.3**	**0.9377 ± 0.0186**	**32.65 ± 2.30**	**0.9156 ± 0.0258**

Note: Data are means ± standard deviations, and the bold values denote which model performed the best under each image metric

ComplexNet complex-valued convolutional neural network, *CS-MRI* compressed sensing MRI, *PSNR* peak signal-to-noise ratio, *R* acceleration rate, *RealNet* real-valued convolutional neural network, *SSIM* structural similarity

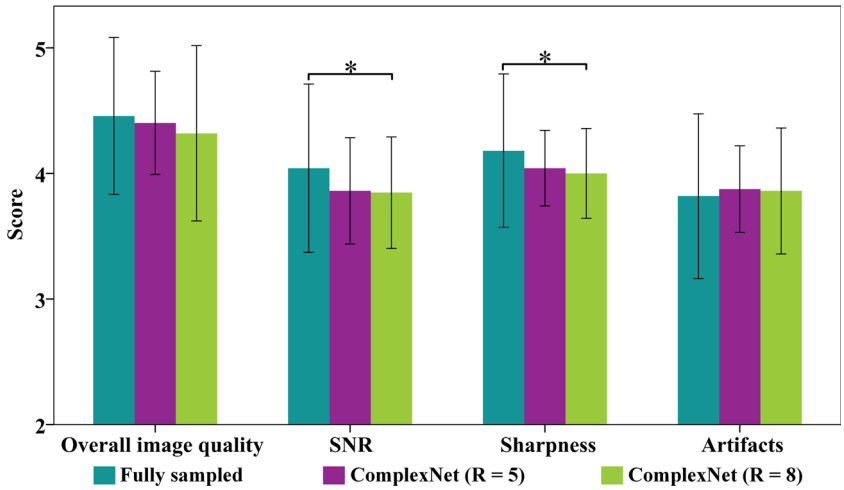

Fig. 3 Quantitative comparisons of image quality scores between the fully sampled and ComplexNet approaches at $R = 5$ and $R = 8$. Image quality scores were evaluated independently by two blinded radiologists in terms of overall image quality, SNR, sharpness, and aliasing artifacts. Bar plots show average scores and their standard deviation across the test data. * denotes statistically different results with $p < 0.05$. *SNR*, signal-to-noise ratio

The comparison of the detection of CMBs between the fully sampled and ComplexNet approaches is shown in Supplementary Table 2. There is no significant difference in the presence or number of CMBs identified on the fully sampled and ComplexNet reconstructed results at both $R = 5$ and $R = 8$ ($p > 0.05$). The interobserver agreement for the presence or number of CMBs following MARS is also excellent in both the fully sampled and ComplexNet reconstructed results (Supplementary Table 3).

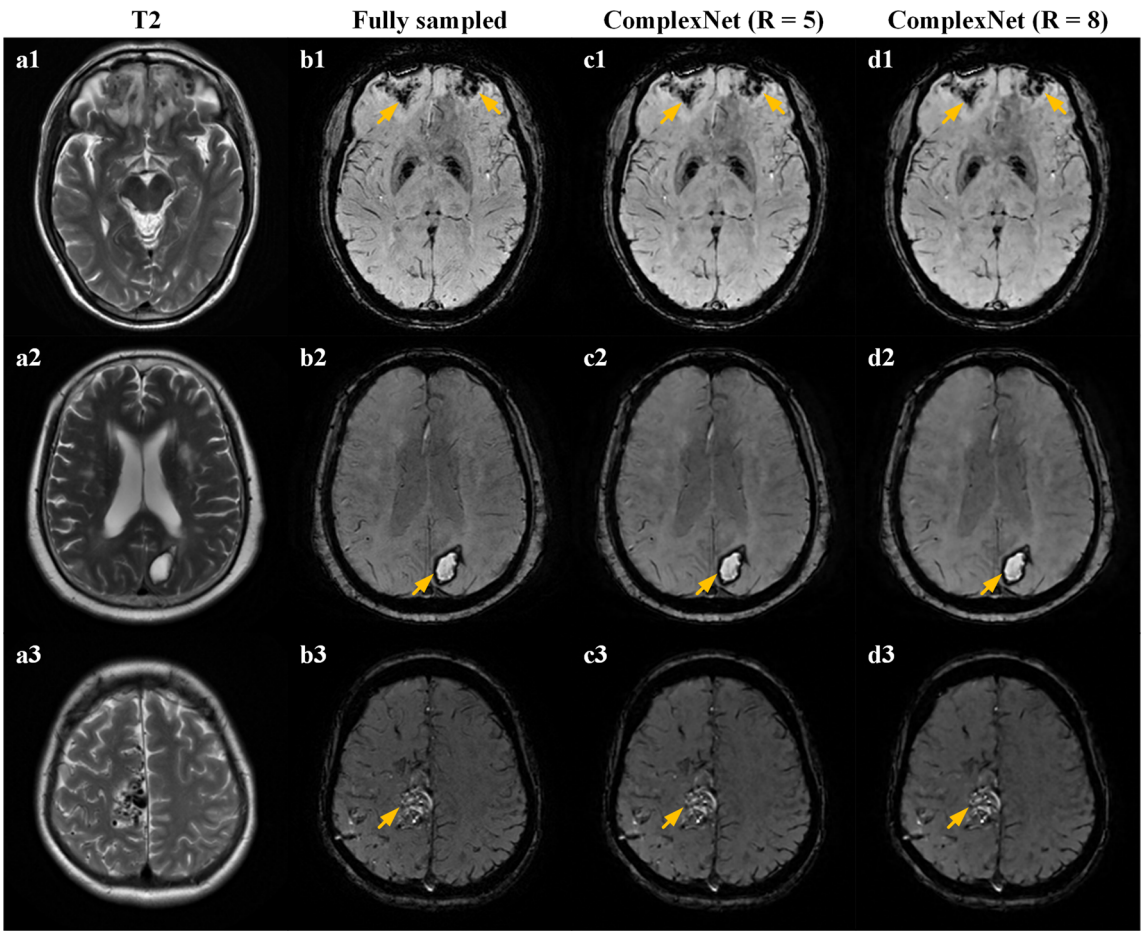

Fig. 4 Representative SWI images comparing the fully sampled and ComplexNet approaches for visualization of pathology, with the T2-weighted MR images (**a1–a3**) shown as reference. **a1–d1** Images in a 61-year-old man with traumatic brain injury. **a2–d2** Images in a 66-year-old woman with cerebral hemorrhage. **a3–d3** Images in a 38-year-old woman with arteriovenous malformation after radiotherapy

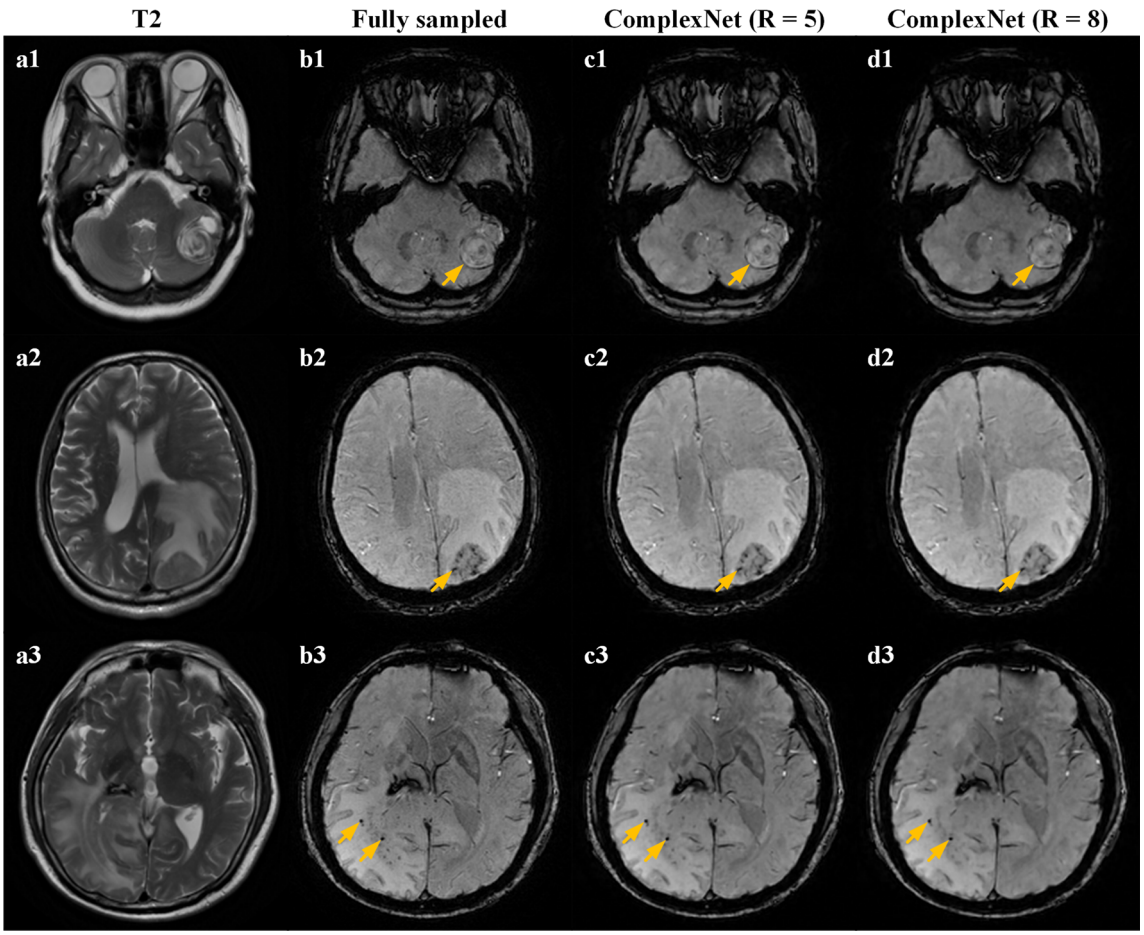

Fig. 5 Representative SWI images show similar diagnostic image quality between fully sampled and ComplexNet approaches, with T2-weighted MR images (**a1–a3**) shown as reference. **a1–d1** Images in a 49-year-old woman with brain tumor. **a2–d2** Images in a 69-year-old man with diffuse large B cell lymphoma. **a3–d3** images in a 49-year-old man with high-grade glioma after biopsy

Discussion

In this study, we developed and clinically evaluated a ComplexNet approach for fast and accurate reconstruction of highly accelerated SWI data. Our results show that ComplexNet can effectively remove undersampled artifacts as well as restore both magnitude and phase images at acceleration rates of 5 and 8. In addition, ComplexNet significantly outperforms the conventional methods in terms of PSNR and SSIM ($p < 0.001$). Furthermore, ComplexNet can provide comparable performance to the fully sampled SWI in terms of overall image quality ($p > 0.05$) and detection of CMBs, with reconstruction speeds of approximately 19 ms per slice, which allows real-time reconstruction of highly accelerated SWI data for practical clinical deployment.

Phase information is critical to many MRI applications, including SWI, quantitative susceptibility mapping, fat-water separation, and phase-contrast imaging [6, 14]. Thus, constructing a network that accurately reconstructs the phase image is highly desirable. Previous studies have demonstrated that complex-valued networks have richer representational power and can more accurately reconstruct the phase image compared to real-valued networks [6]. Therefore, a complex-valued network with unrolled architecture is proposed to faithfully recover both the magnitude and phase images. Our results also show that ComplexNet consistently outperforms RealNet with the same number of trainable parameters regarding quantitative image metrics (Table 2), which is consistent with previous studies [6, 13]. The unrolled network architecture is used in this study because it has been widely used in state-of-the-art MRI reconstruction and has the advantage of incorporating known MR physics [5, 6]. However, the complex-valued framework can be straightforwardly adapted to other network architecture (e.g., U-Net) by replacing the real-valued convolutional layers of existing networks with the complex convolutional layers [6].

Although deep learning has shown great potential in MRI reconstruction, one of the most important concerns of such methods is whether they can faithfully reconstruct abnormalities in clinical practice [27, 28]. Therefore, extensive test data with a wide range of pathology are used to evaluate the performance of ComplexNet. Our study shows that ComplexNet

can provide clear visualization of pathology (Figs. 4 and 5), including hemorrhage, CMBs, and brain tumor, with a five- to eightfold decrease in scan time compared to the fully sampled SWI. The detection of hemorrhage, even a small number of CMBs, is often clinically important in the emergency setting [2]. Therefore, the decreased scan time with ComplexNet is promising to facilitate widely adoption of SWI for time-critical diseases, such as stroke, hemorrhage, and traumatic brain injury [3, 29].

However, patient abnormalities can be quite heterogeneous, and some abnormalities are rare and unlikely to be included in the training data set [28]. In addition, the undersampled MRI reconstruction has intrinsic uncertainty [30, 31]. Therefore, deep learning–based reconstruction methods might remove critical features or create false features that could result in a misdiagnosis [28]. In order to guarantee faithful recovery, the reconstruction model should learn a low-dimensional manifold where the reconstructed images have not only superior sharpness and diagnostic quality, but also consistent with both the real MRI data and the acquisition model [32]. Furthermore, it is also important to quantify and display the pixel-wise reconstruction uncertainty for clinical applications in the future [30, 31]. This could allow radiologists to gain additional insight on the reconstruction quality and potentially generate a better diagnosis outcome [30].

It should be noted that the fine details of some ComplexNet reconstructed images looked slightly smoothed compared to the fully sampled results, which can be further confirmed by the quantitative comparison of sharpness score between the two approaches (Fig. 3). This is most likely due to the use of the mean-squared error loss in the training process, which drives the deep learning model to search pixel-wise averages of plausible solutions [9, 33]. In the future, it will be promising to integrate better learning metrics, such as generative adversarial network [34], perceptual loss [35], to ComplexNet to improve perceptual quality and fine texture details of the reconstruction results.

Our study had several limitations. First, although the enhanced T2*-weighted angiography is a multi-echo GRE sequence, only the GRE data with echo time = 23.0 ms were used to train and evaluate ComplexNet for SWI application. Further evaluation of ComplexNet for R2* mapping and quantitative susceptibility mapping using multi-echo data would be a valuable extension of this study [14]. Second, ComplexNet was only assessed on retrospectively undersampled data and has not been validated on prospective acquisition. In the future, additional evaluation on prospective datasets with variable clinical settings and MRI machines will be performed to further demonstrate the clinical potential of ComplexNet.

In conclusion, the proposed ComplexNet is effective in accelerating the acquisition of SWI data and providing high-quality image reconstruction for visualizing a wide range of pathology. Broader clinical application of ComplexNet may result in more efficient diagnosis and treatment of time-critical diseases.

Supplementary Information The online version contains supplementary material available at https://doi.org/10.1007/s00330-022-08638-1.

Funding This study has received funding by the National Natural Science Foundation of China (81825012, 81730048, 81625011).

Declarations

Ethics approval Institutional Review Board approval was obtained.

Informed Consent Written informed consent was obtained from all subjects (patients) in this study.

Conflict of Interest The authors of this manuscript declare no relationships with any companies whose products or services may be related to the subject matter of the article.

Guarantor The scientific guarantor of this publication is Xin Lou, MD.

Statistics and Biometry One of the authors has significant statistical expertise.

Methodology
- Prospective
- Observational
- Performed at one institution

References

1. Liu C, Li W, Tong KA, Yeom KW, Kuzminski S (2015) Susceptibility-weighted imaging and quantitative susceptibility mapping in the brain. J Magn Reson Imaging 42:23–41
2. Conklin J, Longo MGF, Cauley SF et al (2019) Validation of highly accelerated wave–CAIPI SWI compared with conventional SWI and T2*-weighted gradient recalled-echo for routine clinical brain MRI at 3T. AJNR Am J Neuroradiol 40:2073–2080
3. Haller S, Haacke EM, Thurnher MM, Barkhof F (2021) Susceptibility-weighted imaging: technical essentials and clinical neurologic applications. Radiology 299:3–26
4. Bilgic B, Ye H, Wald LL, Setsompopa K (2017) Simultaneous time interleaved multislice (STIMS) for rapid susceptibility weighted acquisition. Neuroimage 155:577–586
5. Yaman B, Hosseini SAH, Moeller S, Ellermann J, Uğurbil K, Akçakaya M (2020) Self-supervised learning of physics-guided reconstruction neural networks without fully-sampled reference data. Magn Reson Med 84:3172–3191
6. Cole E, Cheng J, Pauly J, Vasanawala S (2021) Analysis of deep complex-valued convolutional neural networks for MRI reconstruction and phase-focused applications. Magn Reson Med 86:1093–1109
7. Chung MS, Lee EJ, Kim S, Kim SO, Byun JS (2020) Wave-CAIPI susceptibility-weighted imaging achieves diagnostic performance comparable to conventional susceptibility-weighted imaging in half the scan time. Eur Radiol 30:2182–2190

8. Chen F, Taviani V, Malkiel I et al (2018) Variable-density single-shot fast spin-echo MRI with deep learning reconstruction by using variational networks. Radiology 289:366–373
9. Duan C, Deng H, Xiao S et al (2019) Fast and accurate reconstruction of human lung gas MRI with deep learning. Magn Reson Med 82:2273–2285
10. Shanbhogue K, Tong A, Smereka P et al (2021) Accelerated single-shot T2-weighted fat-suppressed (FS) MRI of the liver with deep learning–based image reconstruction: qualitative and quantitative comparison of image quality with conventional T2-weighted FS sequence. Eur Radiol. https://doi.org/10.1007/s00330-021-08008-3
11. Dedmari MA, Conjeti S, Estrada S, Ehses P, Stöcker T, Reuter M (2018) Complex fully convolutional neural networks for MR image reconstruction. Proceedings of first international workshop, machine learning for medical image reconstruction (MLMIR), at MICCAI 30–38
12. Wang S, Cheng H, Ying L et al (2020) DeepcomplexMRI: Exploiting deep residual network for fast parallel MR imaging with complex convolution. Magn Reson Imaging 68:136–147
13. El-Rewaidy H, Neisius U, Mancio J et al (2020) Deep complex convolutional network for fast reconstruction of 3D late gadolinium enhancement cardiac MRI. NMR Biomed 33:e4312
14. Gao Y, Cloos M, Liu F, Crozier S, Pike GB, Sun H (2021) Accelerating quantitative susceptibility and R2* mapping using incoherent undersampling and deep neural network reconstruction. Neuroimage 240:118404
15. Sun H, Cleary JO, Glarin R et al (2020) Extracting more for less: multi-echo MP2RAGE for simultaneous T1-weighted imaging, T1 mapping, R_2* mapping, SWI, and QSM from a single acquisition. Magn Reson Med 83:1178–1191
16. Liu F, Samsonov A, Chen L, Kijowski R, Feng L (2019) SANTIS: Sampling-augmented neural network with incoherent structure for MR image reconstruction. Magn Reson Med 82:1890–1904
17. Schlemper J, Caballero J, Hajnal JV, Price AN, Rueckert D (2018) A deep cascade of convolutional neural networks for dynamic MR image reconstruction. IEEE Trans Med Imaging 37:491–503
18. Duan C, Deng H, Xiao S et al (2021) Accelerate gas diffusion-weighted MRI for lung morphometry with deep learning. Eur Radiol. https://doi.org/10.1007/s00330-021-08126-y
19. Kingma DP, Ba J (2014) Adam: a method for stochastic optimization. https://arxiv.org/abs/1412.6980. Accessed 22 Dec 2014
20. Chan KS, Marques JP (2021) SEPIA-susceptibility mapping pipeline tool for phase images. Neuroimage 227:117611
21. Lustig M, Donoho D, Pauly JM (2007) Sparse MRI: the application of compressed sensing for rapid MR imaging. Magn Reson Med 58:1182–1195
22. Wang Z, Bovik AC, Sheikh HR, Simoncelli EP (2004) Image quality assessment: from error visibility to structural similarity. IEEE Trans Image Process 13:600–612
23. Chung MS, Lee EJ, Kim S, Kim SO, Byun JS (2020) Wave-CAIPI susceptibility-weighted imaging achieves diagnostic performance comparable to conventional susceptibility-weighted imaging in half the scan time. Eur Radiol 30:2182–2190
24. Gregoire S, Chaudhary U, Brown M et al (2009) The microbleed anatomical rating scale (MARS) reliability of a tool to map brain microbleeds. Neurology 73:1759–1766
25. Ahn S, Park SH, Lee KH (2013) How to demonstrate similarity by using noninferiority and equivalence statistical testing in radiology research. Radiology 267:328–338
26. Tanenbaum LN, Tsiouris AJ, Johnson AN et al (2017) Synthetic MRI for clinical neuroimaging: results of the magnetic resonance image compilation (MAGiC) prospective, multicenter, multireader trial. AJNR Am J Neuroradiol 38:1103–1110
27. Antun V, Renna F, Poon C, Adcock B, Hansen AC (2020) On instabilities of deep learning in image reconstruction and the potential costs of AI. Proc Natl Acad Sci U S A 117:30088–30095
28. Sandino CM, Cheng JY, Chen F, Mardani M, Pauly JM, Vasanawala SS (2020) Compressed sensing: from research to clinical practice with deep neural networks. IEEE Signal Process Mag 37:111–127
29. Liu S, Buch S, Chen Y et al (2017) Susceptibility-weighted imaging: current status and future directions. NMR Biomed 30:e3552
30. Zhang Z, Romero A, Muckley MJ, Vincent P, Yang L, Drozdzal M (2019) Reducing uncertainty in undersampled MRI reconstruction with active acquisition. Proceedings of the IEEE conference on computer vision and pattern recognition 2049–2058
31. Edupuganti V, Mardani M, Vasanawala S, Pauly J (2020) Uncertainty quantification in deep MRI reconstruction. IEEE Trans Med Imaging 40:239–250
32. Mardani M, Gong E, Cheng JY et al (2018) Deep generative adversarial neural networks for compressive sensing MRI. IEEE Trans Med Imaging 38:167–179
33. Ledig C, Theis L, Huszár F, Caballero J, Cunningham A (2017) Photorealistic single image super-resolution using a generative adversarial network. Proceedings of the IEEE conference on computer vision and pattern recognition 4681–4690
34. Quan TM, Nguyen-Duc T, Jeong WK (2018) Compressed sensing MRI reconstruction using a generative adversarial network with a cyclic loss. IEEE Trans Med Imaging 37:1488–1497
35. Yang Q, Yan P, Zhang Y et al (2018) Low-dose CT image denoising using a generative adversarial network with Wasserstein distance and perceptual loss. IEEE Trans Med Imaging 37:1348–1357